Detecting Dopant Diffusion Enhancement at Grain Boundaries in Multicrystalline Silicon Wafers With Microphotoluminescence Spectroscopy

Hieu T. Nguyen, Sudha Mokkapati, and Daniel Macdonald

***Abstract*—Employing microphotoluminescence spectroscopy at low temperatures, we are able to detect dopant diffusion enhancement along various grain boundaries and subgrain boundaries in multicrystalline silicon wafers. We find an enhancement of phosphorus diffusion at all investigated grain boundary types. In addition, the subgrain boundaries are demonstrated to contain a relatively high density of defects and impurities, suggesting that their presence does not significantly hinder the preferential diffusion of dopant atoms along the subgrain boundaries. Finally, we demonstrate that the technique can be applied to different diffused layers for solar cell applications, even at room temperature if an appropriate excitation wavelength is used. The results are validated with secondary electron dopant contrast images, which confirm the higher dopant concentration along the grain boundaries and subgrain boundaries.**

***Index Terms*—Crystalline silicon, diffusion processes, grain boundaries (GBs), photoluminescence, photovoltaic cells.**

I. Introduction

HOMOGENOUS diffused junctions are important for high-efficiency multicrystalline silicon (mc-Si) solar cells. However, diffusivities of dopant atoms along certain grain boundaries (GBs) have been reported to be higher than in intragrain regions [1]–[7]. Also, when annealed at high temperatures, surrounding dopants are known to be segregated into GBs [8], [9]. These two effects, thus, create deeper and more heavily doped p-n junctions at GBs in mc-Si solar cells. The diffusion enhancement has been studied empirically by many authors using different methods, including beveling and staining [1], electron-beam-induced current (EBIC) [3]–[5], or light-beam-induced current (LBIC) [7] techniques. However, these techniques require not only an angle-lapping or cross-sectioning of the GBs to expose the junctions but also a contact formation to extract the induced current for the case of EBIC and LBIC. Therefore, they are destructive and require complex sample preparation. In addition, phosphorus diffusion has been reported to be enhanced along the so-called small-angle or subgrain boundaries (sub-GBs) by means of beveling and staining [1] or EBIC measurements [5]. However, since sub-GBs often contain high densities of defects and impurities, they are very recombination active. Therefore, investigating the diffusion enhancement along the sub-GBs using EBIC or LBIC is limited, and the interpretation on the experimental results could be potentially affected because the defects/impurities and diffused dopants have opposing impacts on the induced current.

Recently, employing a microphotoluminescence spectroscopy (μ-PLS) system, we demonstrated the separation of luminescence peaks from diffused layers and the underlying silicon substrate at low temperatures [10], courtesy of band gap narrowing effects in heavily doped silicon [11], [12]. In this paper, we apply the technique to detect and study the diffusion enhancement of dopant atoms along large angle GBs and sub-GBs. First, we demonstrate the method with relatively heavy phosphorus-diffused samples whose heavily doped layers are several hundreds of nanometers thick. We find that the diffusion is enhanced for numerous types of large angle GBs, and that sub-GBs also enhance the dopant diffusion, even though they are decorated with a high density of defects and impurities. We, then, discuss the importance of appropriate excitation wavelengths to detect the enhanced diffusion for measurements at room temperature and apply the technique to a light phosphorus diffused sample, whose heavily doped layer is thinner than 100 nm. We find that, even with such light diffusion for standard solar cell applications, the enhanced diffusion still occurs at GBs. Our conclusions are supported by secondary electron images, which confirm the enhanced diffusion along both large angle GBs and sub-GBs. These results highlight the value of this nondestructive, contactless characterization technique in silicon photovoltaics.

II. Experimental Details

The six investigated samples are standard boron-doped p-type mc-Si wafers with a boron doping of about $9 \times 10^{15}\,\mathrm{cm}^{-3}$. First, they were chemically etched in HF/HNO_3 solution to remove saw damage and to achieve polished surfaces. They were then divided into two groups.

The first group consists of two sister wafers consecutively cut from the same ingot. They were immersed in a defect etchant

Manuscript received November 28, 2016; revised January 2, 2017; accepted January 5, 2017. Date of publication January 20, 2017; date of current version February 16, 2017. This work was supported by the Australian Research Council and the Australian Renewable Energy Agency under research Grant RND009.

H. T. Nguyen and D. Macdonald are with the Research School of Engineering, Australian National University, Canberra, ACT 2601, Australia (e-mail: hieu.nguyen@anu.edu.au; daniel.macdonald@anu.edu.au).

S. Mokkapati is with the Department of Electronic Materials Engineering, Australian National University, Canberra, ACT 2601, Australia (e-mail: sudha.mokkapati@anu.edu.au).

Color versions of one or more of the figures in this paper are available online at http://ieeexplore.ieee.org.

Digital Object Identifier 10.1109/JPHOTOV.2017.2650561

TABLE 1
PROCESSING STEPS FOR SIX SAMPLES INVESTIGATED

Processes (in sequence)	Sample A	Sample B	Sample 1	Sample 2	Sample 3	Sample 4
Group number	1	1	2	2	2	2
1. Sister wafer	Yes	Yes	Yes	Yes	Yes	**No**
2. Saw damage etch	Yes	Yes	Yes	Yes	Yes	Yes
3. Defect etch	Yes	Yes	**No**	**No**	Yes	**No**
4. Phosphorus diffusion/Sheet resistance	**No**	Yes/10 $\Omega/\square$	**No**	Yes/10 $\Omega/\square$	Yes/10 $\Omega/\square$	Yes/120 $\Omega/\square$
5. PSG removed by HF	Yes	Yes	Yes	Yes	Yes	Yes

consisting of HF/HNO_3/acetic acid for 16 h to delineate the sub-GBs [13], [14]. One sample was kept in the as-cut state (after the defect etching step). The other sample went through a $POCl_3$ diffusion process at 850°C for 1 h, and then annealed in N_2 gas at 850°C for another 1 h. The resultant sheet resistance was measured on a control float-zone p-type wafer, and was found to be $\sim 10\,\Omega/\square$. The diffused sample was then immersed in HF to remove the phosphosilicate glass (PSG). In Sections III and IV, we perform PL measurements on these two samples mainly at low temperatures in order to unambiguously reveal PL signatures of the enhanced diffusion at GBs, as well as to keep track of the evolution of these signatures versus rising temperatures.

The second group consists of four wafers, three of which were sister wafers in the same ingot. They were either immersed in the defect etchant or skipped this step, and they went through different phosphorus diffusion steps, yielding different sheet resistances. The PSG layers were removed by HF. In Section V, we use these samples to investigate the influence of etch pits (due to the defect etch) on the enhanced diffusion at sub-GBs and of excitation wavelengths. We perform PL measurements only at room temperature in order to demonstrate and discuss capabilities of the μ-PLS technique in practical applications. Table 1 summarizes the processes of all six samples.

The μ-PLS system used here is a Horiba T64000 equipped with a confocal microscope. The excitation source was focused into the sample surface via a 50× objective lens with a numerical aperture of 0.55. The monochromator grating was set at 150 grooves/mm. The emitted PL signal was collected by a liquid-nitrogen-cooled InGaAs array detector. The overall wavelength resolution was 0.25 nm. The spectral response of the entire system was determined with a calibrated halogen–tungsten lamp. The sample temperature was controlled by a liquid-nitrogen-cooled Linkam stage. The cross-sectional surfaces for scanning electron microscope (SEM) analysis were prepared with the focused ion beam (FIB) technique. GB types were determined from electron backscatter diffraction (EBSD) measurements.

Three excitations sources were employed in this paper, two of which were continuous-wave single-frequency lasers of 405 and 532 nm. The other excitation source is a SuperK EXTREME supercontinuum laser with a tunable wavelength range from 490 nm to 2 μm. Due to difficulties in coupling the supercontinuum laser with other lasers in our system, in Sections III and IV, we employ the supercontinuum laser with a wavelength range of 510–810 nm and a bandwidth of 10 nm in order to ensure that the illuminated location is the same with varying excitation wavelengths. Meanwhile, in Section V, we couple the two single-frequency lasers of 405 and 532 nm in order to compare measurements between the two excitation wavelengths on the same illuminated spot. Also, the 532-nm laser has a superior power stability (<1% over 8 h), and thus, allows us to perform μ-PL mappings with a high precision. The on-sample illuminated spot size varied from 1 μm (for 405-nm excitation wavelength) to ~2 μm (for 810-nm excitation wavelength). The on-sample excitation power was kept constant at ~6 mW for all excitation wavelengths.

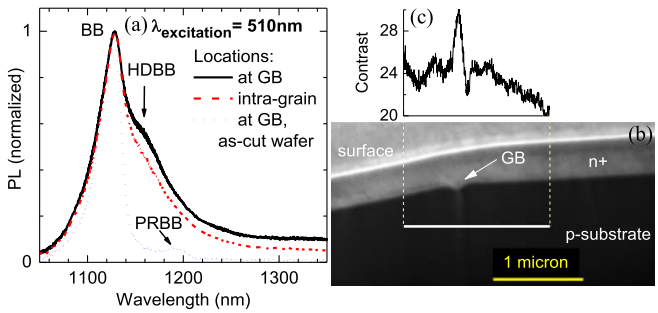

Fig. 1. (a) Normalized PL spectra at a random large angle GB (black line) and in an intragrain region (dashed red line) of the diffused mc-Si wafer (sample B), excited with a 510-nm source at 79 K. The grain misorientation is 53.4° around the [0 1 1] axis. The spectrum at the same GB from the as-cut mc-Si wafer (sample A) is also included for comparison (dotted blue line). (b) Vertical cross-sectional SEM image of the investigated GB of the diffused mc-Si wafer. (c) SE contrast profile of the line scan marked with the white line in (b).

III. ENHANCED DIFFUSION AT LARGE ANGLE GRAIN BOUNDARIES

First, we demonstrate that there are more dopant atoms diffused along GBs than within the intragrain regions. Fig. 1(a) compares the normalized PL spectrum captured at 79 K at a random large angle GB (black curve) with that captured in an intragrain region (dashed red curve) of the diffused mc-Si wafer (sample B), excited with a 510-nm wavelength source. The spectrum at the same GB but from the undiffused as-cut wafer (sample A) is also shown for comparison (dotted blue curve). The main peak located at ~1130 nm is the band-to-band emission (assisted by the emission of a transverse optical phonon) from the underlying Si substrate, and denoted as BB peak. The shoulder located at ~1160 nm is the band-to-band emission (also assisted by the emission of a transverse optical

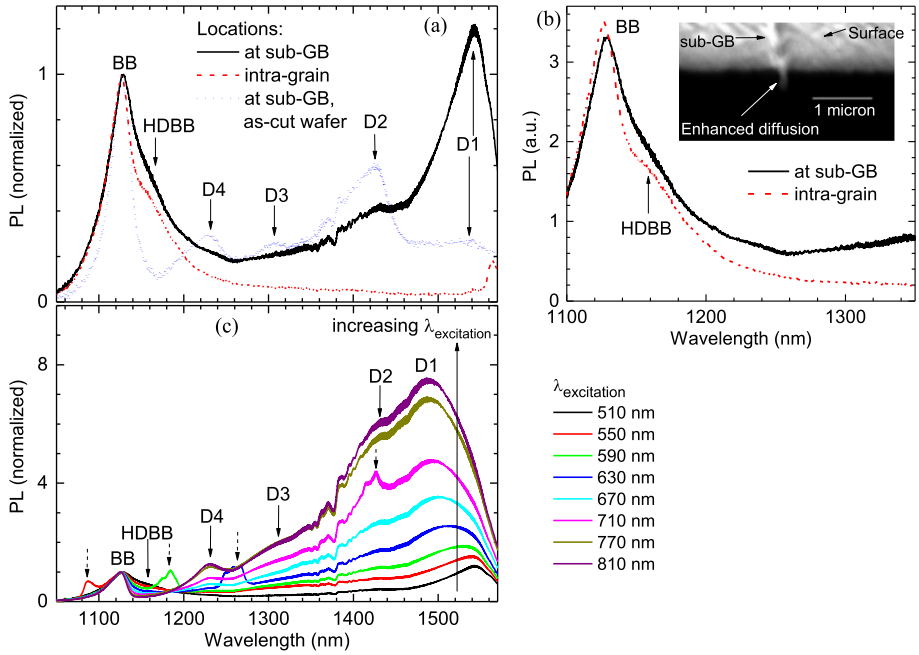

Fig. 2. (a) Normalized and (b) absolute PL spectra at the sub-GB (black line) and the intragrain region (dashed red line) of the diffused mc-Si wafer (sample B), excited with a 510-nm source. The spectrum at the same sub-GB from the as-cut mc-Si wafer (sample A) is also included for comparison (dotted blue line). The inset in b is a vertical cross-sectional SEM image of this sub-GB of the diffused mc-Si wafer. (c) Normalized PL spectra at the sub-GB of the diffused mc-Si wafer with different excitation wavelengths. All measurements were done at 79 K. The normalized spectra were normalized to the band-to-band peak. The spurious peaks marked by broken arrows in (c) are artifacts from the laser light.

phonon) from the heavily doped layer [10], denoted as HDBB peak (heavily doped band-to-band). The HDBB peak captured at the GB is higher than that captured in the intragrain region, suggesting that the GB is more heavily doped than the surrounding regions. The peak around 1200 nm in the spectrum from the as-cut wafer is the phonon-replica of the BB peak, denoted as PRBB (phonon replica of band-to-band). It is the band-to-band emission assisted by the emission of both a transverse optical phonon and an optical zone center phonon.

Fig. 1(b) shows an SEM image of the vertical cross section of the investigated GB. We can observe clearly the contrast difference between the n + diffused layer and the p-type substrate. Compared with the common SEM contrast between n- and p-type Si (brighter for p-type and darker for n-type), the contrast in Fig. 1(b) is inverted (brighter for n + layer and darker for p-substrate) since the cross-sectional surface was contaminated with Ga atoms (whose work function is smaller than that of Si) during the FIB preparation. The mechanism of this contrast inversion was explained in detail in [15]. The contrast profile scan in Fig. 1(c) shows that at the line scan position (about 1 μm below the surface) there are still considerable phosphorus atoms at the GB, i.e., the p-n junction extends much more deeply into the substrate at the GB than in the adjacent regions.

We captured the spectra from numerous large angle GBs including Σ3, Σ5, Σ9, Σ11, Σ27a, and random angle GBs, and always found an enhanced diffusion along these GBs. The results are in contrast with the findings reported in [7], in which the diffusion was shown to be enhanced along Σ3 GBs, but no enhanced diffusion was observed along Σ27a and random large angle GBs. Therefore, a detailed study on the diffusion mechanism of dopant atoms along different types of GBs under various conditions is required to clarify these uncertainties, and this contactless and nondestructive PLS-based method could be a powerful tool to study this diffusion mechanism without complex sample preparation.

IV. Enhanced Diffusion at Sub-Grain Boundaries

Now, we investigate the distribution of dopant atoms around sub-GBs in mc-Si wafers after the phosphorus diffusion step. Sub-GBs contain a high density of dislocations due to the high thermal stress and strain during the ingot growing and cooling. Also, they are often decorated with secondary defects and impurities trapped by the dislocation networks. The dislocations themselves are known to emit two distinct deep-level PL peaks (the so-called D3 and D4 lines), whereas the surrounding secondary defects and impurities emit another two deep-level peaks (D1 and D2 lines) [16]–[20]. First, we examine sub-GBs at which the density of decorating defects and impurities is high. A typical PL spectrum at this kind of sub-GBs from the as-cut mc-Si wafer is given in Fig. 2(a) (dotted blue curve). Besides the D3 and D4 peaks emitted from dislocations, the sub-GB also emits the D1 and D2 peaks due to decorating defects and impurities. Fig. 2(a) and (b) compares the normalized and ab-

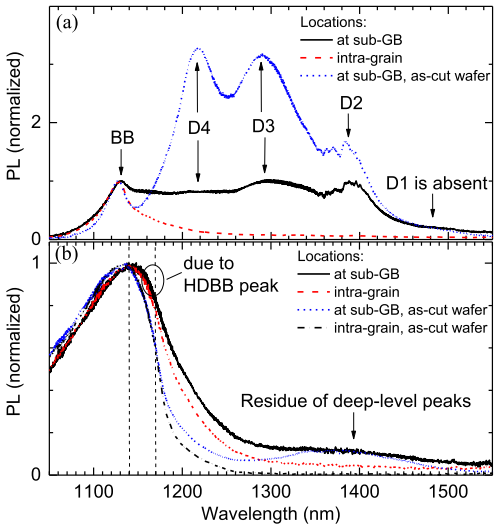

Fig. 3. Normalized PL spectra at another sub-GB (black line) and in an intragrain region (dashed red line) of the diffused mc-Si wafer at (a) 79 K and (b) 300 K, excited with the 510-nm wavelength. The spectra at the same sub-GB (dotted blue lines) and in the intra-grain region (dashed dotted black line) from the as-cut mc-Si wafer were also included for comparisons. The region between the two broken vertical lines is not affected by the deep-level luminescence but affected by the HDBB peak. The normalized spectra were normalized to the band-to-band peak.

solute PL spectra, respectively, of the diffused mc-Si wafer at 79 K, captured at the same sub-GB (black line) and the intragrain region (dashed red line). The intensity (both in normalized and absolute scales) of the HDBB peak at the sub-GB is higher than that in the intragrain region, although the absolute BB intensity at the sub-GB is lower than that in the intragrain region. The results suggest that there are more active dopant atoms along the sub-GB than the intragrain regions. The dopant atoms are still preferentially diffused into the sub-GB even though there is a high density of defects and impurities around it. We note that although the D4 luminescence peak does partly overlap with the HDBB shoulder, making the comparison with the spectra measured away from the sub-GB more difficult, in this case, the magnitude of the D4 luminescence is small enough to still conclude that there is an increased dopant concentration at the sub-GB. To fortify this conclusion, an SEM dopant contrast image was captured on a vertical cross section of this sub-GB of the diffused wafer and is displayed as an inset in Fig. 2(b). The p-n junction clearly extends more deeply into the substrate at the sub-GB than the surrounding regions. In addition, Fig. 2(c) shows the evolution of normalized PL spectra with increasing excitation wavelengths captured at the sub-GB of the diffused wafer at 79 K. In Fig. 2(c), the longer the excitation wavelength, the higher the intensities of the D lines. The results confirm that the defects (both intrinsic dislocations and secondary defects) and impurities are distributed deeply across the wafer thickness rather than being limited to the near-surface region.

Furthermore, we continue investigating sub-GBs that contain dislocations but a relatively low density of secondary defects and impurities and, thus, emit strong D3 and D4 but minimal D1 and D2 lines [20]. Fig. 3(a) and (b) compares the normalized PL spectra captured at a sub-GB (black curve) and in an intragrain region (dashed red curve) of the diffused mc-Si wafer at 79 and 300 K, respectively. The spectra at the same sub-GB but from the as-cut wafer are also presented for comparison. In Fig. 3(a), due to the intense D4 line, it is not possible to observe the HDBB shoulder at low temperatures. However, since the D3 and D4 lines display a strong thermal quenching rate [21]–[23], at room temperature, these two lines are quenched significantly and the contribution of the HDBB peak into the total spectra is more obvious, as depicted in Fig. 3(b). As can be clearly seen from Fig. 3(b), between 1140–1170 nm, the spectra from the as-cut wafer at and away from the sub-GB is not affected by the deep-level peaks. Nevertheless, the shoulder between 1140–1170 nm (due to the HDBB peak) of the spectrum captured at the sub-GB (of the diffused wafer) is still broader than that captured at the intragrain region. The results suggest that more dopants have diffused into this sub-GB than the surrounding regions. Note that the carrier profile and surface reflectivity have a negligible impact on the PL spectral shape at the long wavelength side since reabsorption of the generated photons is negligible at these wavelengths, as demonstrated in [24].

V. Detection of Enhanced Diffusion with Measurements at Room Temperature

In this section, we perform PL measurements only at room temperature in order to demonstrate and discuss capabilities of the μ-PLS technique in practical applications. In fact, we can utilize the spectral properties in Fig. 3(b) to qualitatively assess both the dopant enhancement and the recombination activity around sub-GBs and large angle GBs even at room temperature.

Fig. 4 plots the PL intensity mappings around a sub-GB of the three sister mc-Si wafers excited with the 532-nm wavelength at room temperature. Respectively, Fig. 4(a)–(c) is the integrated PL intensities from 1050 to 1200 nm (absolute intensity), from 1140 to 1160 nm (after spectra were normalized to the BB peak), and from 1200 to 1250 nm (after spectra were normalized to the BB peak). From Fig. 4(a), we can conclude that the sub-GB is recombination active due to a reduction of the integrated band-to-band PL signal (absolute intensity from 1050 to 1200 nm). From Fig. 4(b.2) and (b.3), we can conclude that there are more dopant atoms diffused into the sub-GB than the surrounding region. The reason is that, at room temperature, the broader shoulder between 1140–1160 nm of the normalized spectrum is affected by the HDBB peak emitted from the diffused layer, not by the deep-level luminescence peaks, as demonstrated in Fig. 3(b). Meanwhile, the mapping from the as-cut wafer [see Fig. 4(b.1)] does not show any feature since there is no diffused layer on the as-cut wafer. However, all three samples show a brighter line along the sub-GB in Fig. 4(c). This brighter line is due to both the deep-level luminescence and the HDBB peak since between 1200–1250 nm, there are significant impacts of the deep-level peaks on the PL spectral shape, as can be observed clearly in Fig. 3(b). The results from these images confirm that, although the recombination activity is increased along the sub GB, more dopant atoms are also diffused into the sub-GB, and the etch pits after defect etching do not affect the preferential diffusion of dopants along the sub-GB. These conclusions are more

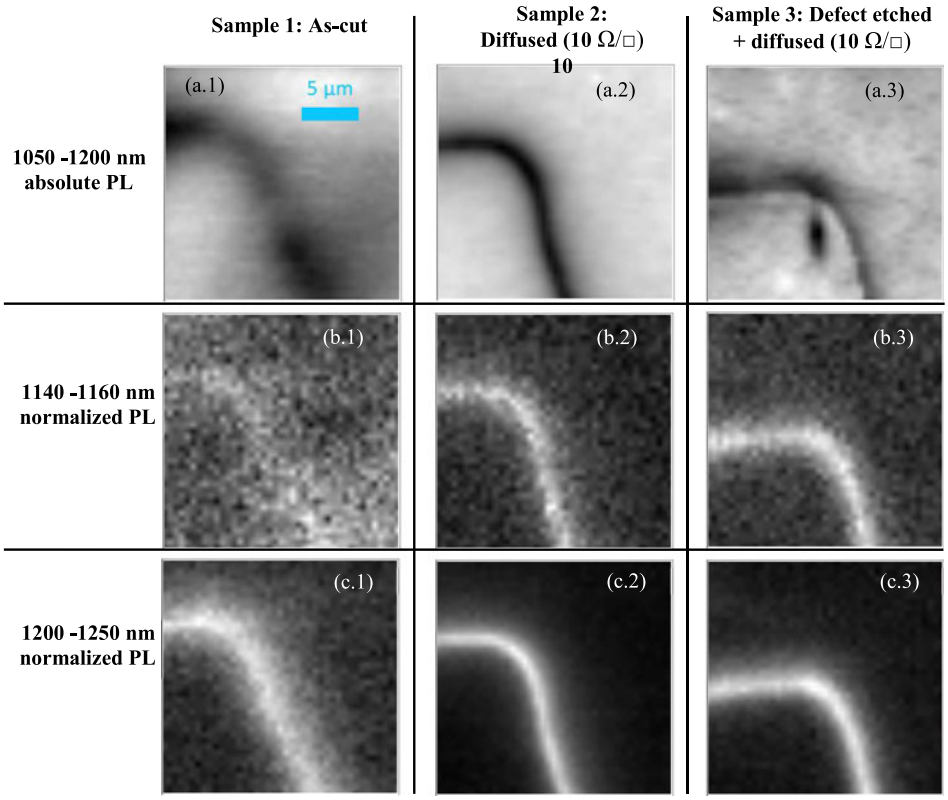

Fig. 4. Mappings of PL intensity at the same sub-GB of 1) sample 1, 2) sample 2, and 3) sample 3. (a) Integrated absolute PL intensity from 1050 to 1200 nm. (b) Integrated PL intensity from 1140 to 1160 nm after spectra were normalized to the BB peak. (c) Integrated PL intensity from 1200 to 1250 nm after spectra was normalized to the BB peak. All measurements were performed at room temperature with the 532-nm excitation wavelength. The scanning step is 0.5 μm in both X and Y directions. The brighter color indicates the higher intensity.

difficult to be made based on EBIC or LBIC measurements since the total induced current is determined by both the defect/impurity and dopant concentrations. The defects and impurities reduce the current, whereas the dopants act to increase it.

Finally, we demonstrate the importance of employing appropriate excitation wavelengths to detect the enhanced diffusion for various phosphorus diffusion conditions at room temperature. We illustrate with two common excitation light sources, 532- and 405 nm. The absorption depths of 532- and 405-nm excitation lights are approximately 1 μm and 100 nm in slightly doped Si, respectively [25], [26]. These values are expected to be smaller in heavily doped Si due to the smaller effective band gap. If the diffusion is too heavy, although the impact of dopants on the PL spectra is more obvious with the 405-nm excitation light than the 532-nm excitation light, we may not be able to detect the enhanced diffusion at GBs with the 405-nm excitation source since the light will be mostly absorbed in the first 100 nm of the heavily doped layer. On the other hand, if the diffusion is too light, the PL signal, captured with the 532-nm excitation source, from the heavily doped layer may not be sufficient in order to reveal the enhanced diffusion.

In fact, Fig. 5(a) compares the normalized PL spectra captured with the 532- and 405-nm excitation sources from sample 2 (heavy diffusion with a sheet resistance of 10 Ω/□) at room temperature. In this figure, we are able to observe the enhanced diffusion at the GB with the 532-nm laser since the longer

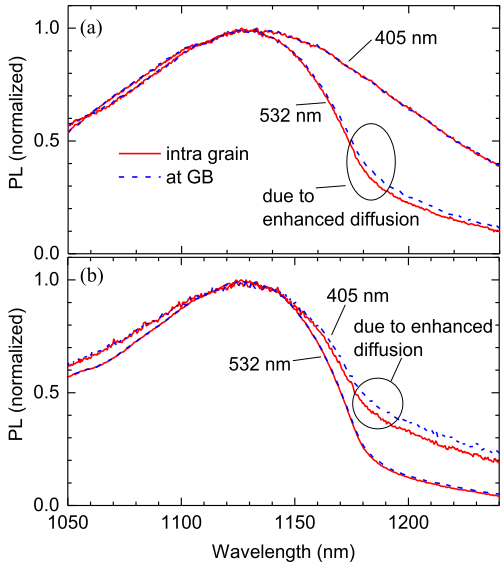

Fig. 5. Comparison of normalized PL spectra between 532- and 405-nm excitation lights at a GB and in the intragrain region, measured at room temperature. (a) Sample 2, heavy phosphorus diffusion with a sheet resistance of 10 Ω/□. (b) Sample 4, light phosphorus diffusion with a sheet resistance of 120 Ω/□.

wavelength side of the spectrum at the GB is broader than that in the intragrain region. Meanwhile, the two spectra (both at GB and in intragrain region) captured with the 405-nm laser are

identical. On the other hand, Fig. 5(b) compares the normalized PL spectra from sample 4 at room temperature. The diffusion condition of this sample is a standard phosphorus diffusion process for p-type mc-Si solar cells. The resultant sheet resistance is 120 Ω/□. Therefore, the heavily doped layer is expected to be very thin ($\sim$100 nm). In Fig. 5(b), the two spectra captured with the 532-nm laser are almost overlapped, whereas the two spectra captured with the 405-nm laser show an obvious difference at the long-wavelength side, suggesting an enhanced diffusion at the GB of sample 4. Therefore, an appropriate excitation wavelength is a critical requirement in order to apply the presented method at room temperature; and for standard photovoltaic applications, a 405-nm excitation source could be more effective than a 532-nm source.

VI. Summary

In conclusion, applying μ-PLS techniques, we have detected dopant diffusion enhancement along GBs and sub-GB in mc-Si wafers. We have demonstrated that this enhancement occurs at numerous types of GBs, rather than only at some specific GBs. In addition, we have shown that the presence of defects and impurities around sub-GBs does not significantly hinder the preferential diffusion of dopant atoms. Finally, we demonstrate the technique to detect the diffusion enhancement at GBs at room temperature, as well as the importance of appropriate excitation wavelengths. These findings help demonstrate the value of such spectrally resolved PL techniques in silicon photovoltaics.

Acknowledgment

The authors would like to thank Prof. H. Tan for providing access to the spectroscopic equipment, T. Duong and Dr. S. P. Phang for assisting with the sample preparation, and Dr. H. C. Sio for helping with the EBSD measurements.

References

[1] H. J. Queisser, K. Hubner, and W. Shockley, "Diffusion along small-angle grain boundaries in silicon," *Phys. Rev.*, vol. 123, pp. 1245–1254, 1961.
[2] A. D. Le Claire, "The analysis of grain boundary diffusion measurements," *Brit. J. Appl. Phys.*, vol. 14, pp. 351–356, 1963.
[3] P. H. Holloway, "Grain boundary diffusion of phosphorus in polycrystalline silicon," *J. Vacuum Sci. Technol.*, vol. 21, pp. 19–22, 1982.
[4] A. D. Buonaquisti, W. Carter, and P. H. Holloway, "Diffusion characteristics of boron and phosphorus in polycrystalline silicon," *Thin Solid Films*, vol. 100, pp. 235–248, 1983.
[5] K. Schimpf, J. Palm, and H. Alexander, "Enhanced diffusion of phosphorus at grain boundaries in multicrystalline silicon," *Cryst. Res. Technol.*, vol. 29, pp. 1123–1129, 1994.
[6] Y. Mishin and Chr. Herzig, "Grain boundary diffusion: Recent progress and future research," *Mater. Sci. Eng. A.*, vol. 260, pp. 55–71, 1999.
[7] M. Breitwieser *et al.*, "Analysis of solar cell cross sections with micro-light beam induced current (μLBIC)," *Solar Energy Mater. Solar Cells*, vol. 131, pp. 124–128, 2014.
[8] A. Carabelas, D. Nobili, and S. Solmi, "Grain boundary segregation in silicon heavily doped with phosphorus and arsenic," *J. Phys. Colloques*, vol. 43, pp. C1-187–C1-192, 1982.
[9] A. Broniatowski, "Electrical measurement of the dopant segregation profile at the grain boundary in silicon bicrystals," *J. Appl. Phys.*, vol. 64, pp. 4516–4525, 1988.
[10] H. T. Nguyen *et al.*, "Micro-photoluminescence spectroscopy on heavily-doped layers of silicon solar cells," *Phys. Status Solidi RRL*, vol. 9, pp. 230–235, 2015.
[11] J. Wagner, "Photoluminescence and excitation spectroscopy in heavily doped n- and p-type silicon," *Phys. Rev. B*, vol. 29, pp. 2002–2009, 1984.
[12] J. Wagner, "Band-gap narrowing in heavily doped silicon at 20 and 300 K studied by photoluminescence," *Phys. Rev. B*, vol. 32, pp. 1323–1325, 1985.
[13] W. C. Dash, "Copper precipitation on dislocations in silicon," *J. Appl. Phys.*, vol. 27, pp. 1193–1195, 1956.
[14] Y. Kashigawa, R. Shimokawa, and M. Yamanaka, "Highly sensitive etchants for delineation of defects in single- and polycrystalline silicon materials," *J. Electrochem. Soc.*, vol. 143, pp. 4079–4087, 1996.
[15] M. El-Gomati, F. Zaggout, H. Jayacody, S. Tear, and K. Wilson, "Why is it possible to detect doped regions of semiconductors in low voltage SEM: A review and update," *Surface Interface Anal.*, vol. 37, pp. 901–911, 2005.
[16] S. Binetti *et al.*, "Optical properties of oxygen precipitates and dislocations in silicon," *J. Appl. Phys.*, vol. 92, pp. 2437–2445, 2002.
[17] M. Tajima *et al.*, "Deep-level photoluminescence due to dislocations and oxygen precipitates in multicrystalline Si," *J. Appl. Phys.*, vol. 111, pp. 113523-1–113523-6, 2012.
[18] M. Tajima, "Spectroscopy and topography of deep-level luminescence in photovoltaic silicon," *IEEE J. Photovolt.*, vol. 4, no. 6, pp. 1452–1458, Nov. 2014.
[19] S. Binetti, A. Le Donne, and A. Sassella, "Photoluminescence and infrared spectroscopy for the study of defects in silicon for photovoltaic applications," *Solar Energy Mater. Solar Cells*, vol. 130, pp. 696–703, 2014.
[20] H. T. Nguyen, F. E. Rougieux, F. Wang, H. Tan, and D. Macdonald, "Micrometer-scale deep-level spectral photoluminescence from dislocations in multicrystalline silicon," *IEEE J. Photovolt.*, vol. 5, no. 3, pp. 799–804, Mar. 2015.
[21] M. Suezawa, Y. Sasaki, and K. Sumino, "Dependence of photoluminescence on temperature in dislocated silicon crystals," *Phys. Status Solidi A*, vol. 79, pp. 173–181, 1983.
[22] R. Sauer *et al.*, "Dislocation-related photoluminescence in silicon," *Appl. Phys. A*, vol. 36, pp.1–13, 1985.
[23] V. V. Kveder, E. A. Steinman, S. A. Shevchenko, and H. G. Grimmeiss, "Dislocation-related electroluminescence at room temperature in plastically deformed silicon," *Phys. Rev. B*, vol. 51, pp. 10520–10526, 1995.
[24] H. T. Nguyen, F. E. Rougieux, S. C. Baker-Finch, and D. Macdonald, "Impact of carrier profile and rear-side reflection on photoluminescence spectra in planar crystalline silicon wafers at different temperatures," *IEEE J. Photovolt.*, vol. 5, no. 1, pp. 77–81, Jan 2015.
[25] M. A. Green, "Self-consistent optical parameters of intrinsic silicon at 300 K including temperature coefficients," *Solar Energy Mater. Solar Cells*, vol. 92, pp. 1305–1310, 2008.
[26] C. Schinke *et al.*, "Uncertainty analysis for the coefficient of band-to-band absorption of crystalline silicon," *AIP Adv.*, vol. 5, 2015, Art. no. 067168.

Authors' photographs and biographies not available at the time of publication.